Structural Organization of the Ni and (4Fe-4S) Centers in the Active Form of *Desulfovibrio gigas* Hydrogenase. Analysis of the Magnetic Interactions by Electron Paramagnetic Resonance Spectroscopy†

Bruno Guigliarelli,*,‡ Claude More,‡ André Fournel,‡ Marcel Asso,‡ E. Claude Hatchikian,§ Ruth Williams,|| Richard Cammack,|| and Patrick Bertrand‡

Laboratoire d'Electronique des Milieux Condensés and UPR-CNRS 9036, Université de Provence, Centre de St-Jérôme, 13397 Marseille cedex 20, France, Bioénergétique et Ingénierie des Protéines, UPR 9036 CNRS, 31 chemin J. Aiguier, 13402 Marseille cedex 09, France, and Division of Life Sciences, King's College, London W8 7AH, U.K.

Received November 14, 1994⊗

ABSTRACT: The *Desulfovibrio gigas* hydrogenase is a typical (NiFe) hydrogenase containing a Ni center and three FeS centers, one [3Fe-4S] and two [4Fe-4S] clusters. When the enzyme is activated under hydrogen gas, the Ni center becomes paramagnetic, giving a characteristic electron paramagnetic resonance (EPR) signal with g values at 2.19, 2.14 and 2.01, the Ni−C signal. Two redox states of the enzyme can be prepared, in which the [4Fe-4S] clusters are either diamagnetic or paramagnetic. In this latter state, the magnetic coupling between metal centers induces both the appearance at low temperature of a complex EPR spectrum, the split Ni−C signal, and a significant enhancement of the relaxation rates of the Ni center. Good simulations of the split Ni−C signal recorded at three different microwave frequencies (X-band, Q-band, and S-band) are obtained by using a model based on a point dipole approximation of the dipolar and exchange interactions between paramagnets. The spectral analysis demonstrates that only one $[4Fe\text{-}4S]^{1+}$ cluster is significantly coupled to the Ni site and provides a detailed description of the relative arrangement of the two centers. In addition, the magnetic characteristics of this $[4Fe\text{-}4S]^{1+}$ cluster can be deduced from the simulations. Moreover, the spin−spin and spin−lattice relaxation times of the interacting centers were measured in the two redox states of the enzyme, either by power saturation and pulsed EPR experiments at low temperature or from the broadening of the EPR lines at higher temperature. The relaxation behavior of the Ni center is well explained by using in the theoretical analysis, the set of structural and magnetic parameters deduced from the spectral simulations. Our structural conclusions on the active *D. gigas* hydrogenase are compared to the preliminary data of a low-resolution crystal structure of the oxidized enzyme [Volbeda, A., Piras, C., Charon, M. H., Hatchikian, E. C., Frey, M., & Fontecilla-Camps, J. C. (1993) *News Lett. Protein Crystallogr. 28,* 30−33].

Hydrogenases are enzymes involved in the production and consumption of molecular hydrogen by microorganisms. Two types of enzymes have been distinguished according to their metal content, the [Fe] only (Adams, 1990) and [NiFe] hydrogenases (Cammack, 1992). The periplasmic hydrogenase from the sulfate-reducing bacterium *Desulfovibrio gigas* is one of the best-studied enzymes of the [NiFe] class (Hatchikian et al., 1990). This enzyme is composed of two subunits of approximately 60 and 28 kDa and contains four metal centers: one Ni center, which is considered to be the activation site of hydrogenase, and three iron−sulfur centers (one [3Fe-4S] and two [4Fe-4S] clusters), which are likely involved in the electron exchange between the catalytic site and the redox partners of the enzyme (Hatchikian et al., 1990).

D. gigas hydrogenase can be prepared in several redox states, which have been thoroughly investigated by electron paramagnetic resonance (EPR) spectroscopy (Cammack et al., 1982; LeGall et al., 1982; Teixeira et al., 1983, 1985, 1989; Fernandez et al., 1986; Cammack et al., 1987). The EPR spectrum of the oxidized form of the enzyme shows the superposition of a nearly isotropic $[3Fe\text{-}4S]^{1+}$ signal centered at $g = 2.01$ with two rhombic signals attributed to Ni(III) centers, the Ni-A signal with g-values equal to 2.32, 2.23, and 2.01 and the Ni-B signal with g-values equal to 2.34, 2.16, and 2.01. The Ni-B signal is associated with a "ready state" of the enzyme which can rapidly become active on reduction, whereas the Ni-A signal corresponds to an "unready state" requiring a prolonged incubation with reductants to recover the catalytic activity (Teixeira et al., 1985; Fernandez et al., 1986). Upon reduction of the enzyme, these signals disappear and a new nickel signal appears at $g = 2.19$, 2.14, and 2.01. This signal is termed the Ni−C signal and is believed to correspond to an active form of the enzyme (Fernandez et al., 1986). It is light-sensitive, being transformed upon illumination into the Ni−C* signal (Cammack et al., 1987). The strong isotopic effect observed with ^2H_2O in the photoconversion of the Ni−C signal in the hydrogenase of *Chromatium vinosum* (Van der Zwaan et al., 1985) strongly suggests that this signal arises from a hydrogenated species of Ni involved in the reaction cycle of hydrogenase. Upon further reduction of the enzyme, the [4Fe-4S] clusters become paramagnetic and interact

† This work was supported in part by the Alliance Anglo-French joint research program, 92094, and by a grant to R.C. from the U.K. Science and Engineering Research Council.

* Corresponding author.
‡ Université de Provence.
§ Bioénergétique et Ingénierie des Protéines, UPR 9036 CNRS.
|| King's College.

⊗ Abstract published in *Advance ACS Abstracts,* March 1, 1995.

0006-2960/95/0434-4781$09.00/0

magnetically with the Ni center. This interaction changes the Ni−C signal into a complex EPR spectrum, the so-called split Ni−C signal, only visible at low temperature (Cammack et al., 1987; Teixeira et al., 1989). Other [NiFe] hydrogenases that have been investigated show essentially the same redox behavior, with small variations of the midpoint potentials and of the *g*-values of the paramagnetic species (Coremans et al., 1992; Asso et al., 1992; Cammack et al., 1989; Hatchikian et al., 1990; Franco et al., 1993). The most important differences are observed for the [NiFeSe] hydrogenases, which lack the [3Fe-4S] cluster and have selenium coordinated to the Ni site (Teixeira et al., 1987).

To date, the coordination of the Ni center in the different redox states of the enzyme is not completely elucidated and only tentative models have been proposed (Albracht et al., 1984; Hatchikian et al., 1990; Sorgenfrei et al., 1993). Extended X-ray absorption fine structure (EXAFS) experiments carried out on various [NiFe] hydrogenases indicated that the Ni site is five- or six-coordinate with 2−4 sulfur ligands, the other ligands being nitrogen or oxygen atoms (Lindhal et al., 1984; Scott et al., 1984; Bagyingka et al., 1993). Electron spin−echo envelope modulation (ESEEM) experiments have also shown the presence of a nitrogen atom in the vicinity of the Ni site, but due to the weakness of the hyperfine interaction, it was not possible to conclude whether or not this nitrogen atom is directly bound to the Ni ion (Tan et al., 1984; Chapman et al., 1988). Moreover, nickel-substituted rubredoxins, in which the native iron atom was replaced by a nickel ion in a distorted tetrahedral coordination of cysteine residues, showed catalytic (Saint-Martin et al., 1988) and spectroscopic properties (Mus-Veteau et al., 1991) similar to those of hydrogenases. These observations support the presence of several sulfur ligands in the coordination shell of the Ni site of hydrogenases.

A limited amount of structural information has been provided by amino acid sequence comparisons (Voordouw, 1992). It has been proposed that the conserved motif Cys-x-x-Cys-x-x-His located in the C-terminal part of the large subunit (60 kDa) is involved in the binding of Ni. This proposal is supported by the fact that the first Cys residue of this motif is replaced by a selenocysteine in [NiFeSe] hydrogenase (Voordouw et al., 1989), and selenium is a ligand to the nickel atom in these enzymes (He et al., 1989; Sorgenfrei et al., 1993). A second conserved motif Cys-x-x-Cys-x-x-x-His is present in the N-terminal region of the large subunit and could also be involved in Ni coordination (Mus-Veteau et al., 1991; Hatchikian et al., 1990). Moreover, the small subunit contains 10 conserved cysteines, which probably bind some Fe−S clusters but are not sufficient to coordinate all the hydrogenase FeS centers. Thus, in spite of many studies devoted to [NiFe] hydrogenases, the location of the metal centers within the enzyme and their structural organization is not clear.

The presence of magnetic interactions between the reduced $[4Fe\text{-}4S]^{1+}$ clusters and the Ni site in the active state of *D. gigas* hydrogenase provides a good opportunity to gain such structural information. Magnetic interactions between paramagnetic groups are frequently observed in multisite redox enzymes (Cammack et al., 1994), and depending on the relative electron spin relaxation properties of the interacting centers, they may lead to an enhancement of the relaxation rates of the paramagnetic and/or the appearance of complex EPR spectra. Recent studies have demonstrated that the analysis of the relaxation properties (Hirsh et al., 1992) and the simulation of complex EPR spectra (Guigliarelli et al., 1993; Bertrand et al., 1994) are powerful methods to determine the structural arrangement of paramagnetic centers at distances of about 0.5−2.5 nm.

In this paper, both approaches have been applied in order to rationalize the magnetic properties of the Ni−C state. The split Ni−C signal, which is due to spin−spin interactions between the Ni−C site and the $[4Fe\text{-}4S]^{1+}$ clusters, has then been recorded at three different microwave frequencies, at S-band (4 GHz), X-band (9 GHz), and Q-band (35 GHz). Good simulations of this signal were obtained at these three frequencies by using the same set of magnetic and structural parameters. Moreover, spin−spin and spin−lattice relaxation times of the Ni center were measured in two redox states of the enzyme, in which the [4Fe-4S] clusters were either diamagnetic or paramagnetic. Depending on the temperature range, pulsed EPR experiments, microwave power saturation, or line broadening studies were used for these measurements. The relaxation behavior of the Ni center was well explained by a theoretical analysis using the set of parameters deduced from the spectral simulations.

All these results are consistent with the magnetic interaction of only one $[4Fe\text{-}4S]^{1+}$ cluster with the Ni center in the active form of the enzyme, and they provide a detailed description of the relative arrangement of the two centers. This structural information is discussed in connection with the preliminary data given by a low-resolution crystal structure of *D. gigas* hydrogenase (Volbeda et al., 1993).

MATERIALS AND METHODS

Biological Samples. *D. gigas* hydrogenase was purified as previously described (Hatchikian et al., 1978). The enzyme was concentrated on Amicon Centricon concentrators to a final volume of 100 μL and concentration 3.2 mM, in 0.1 M 2-(*N*-morpholino)ethanesulfonate buffer, pH 6.5. The potential was poised by reduction with hydrogen in an electrochemical cell designed for preparation of small-volume EPR samples (Cammack & Cooper, 1993). The cell was purged with water-saturated hydrogen and argon gas, as previously described (Cammack, 1987). In order to avoid free radical signals at $g = 2.00$, no mediators were added. The platinum electrode responded directly to the concentration of hydrogen in solution, with which the enzyme was in equilibrium. In order to convert the enzyme to the "active" state, giving the Ni−C EPR signal (Fernandez et al., 1985), the enzyme was activated by incubation at 20 °C under hydrogen for 15 h. Samples of Ni−C for EPR spectroscopy were prepared in Q-band quartz tubes of 2 mm internal diameter. For a sample giving predominantly the unsplit Ni−C signal, the sample was purged with argon, with stirring, for 15 min. When the potential reading was −354 mV vs the standard hydrogen electrode, a 40-μL sample was transferred anaerobically, with a gastight syringe, into the quartz Q-band sample tube, previously purged with hydrogen. The tube was frozen in a methanol freezing bath, removed from the apparatus, and stored in liquid nitrogen. For the sample of enzyme giving the split Ni−C signal, the remainder of the protein was purged with hydrogen for 5 min, and a sample was taken at a recorded potential of −376 mV. EPR spectra were taken of the samples as they were prepared, in order to monitor the redox state of the protein.

EPR Spectroscopy. X-band spectra were recorded on a Bruker ESP300 spectrometer equipped with the ESP 1620 data processing unit. The samples were cooled by an Air-Product Helitran gas flow system or by an Oxford Instrument ESR 900 cryostat with a ITC4 temperature controller. Q-band spectra were obtained on a Varian E 112 spectrometer equipped with a Varian E 110 microwave bridge. Cooling of the sample was performed with an Oxford Instrument CF 35 cryostat. S-band spectra were recorded on a Bruker ESP 300 spectrometer equipped with an ER061SR microwave bridge and fitted with an CF935 Oxford cryostat.

Numerical Simulation. Spectral simulations were performed by using the computer program POINTDIP recently developed by some of us (Guigliarelli et al., 1993) to describe the magnetic interactions between two paramagnetic point dipoles A and B with spins $S_A = S_B = {}^1/_2$. This program is based on the numerical diagonalization of the spin Hamiltonians

$$H = H_z + H_{ex} + H_{dip} \tag{1}$$

with

$$H_z = \beta \vec{B}\, \mathbf{g}_A \vec{S}_A + \beta \vec{B}\, \mathbf{g}_B \vec{S}_B \tag{2}$$

$$H_{ex} = -2\, \vec{S}_A \mathbf{J} \vec{S}_B \tag{3}$$

$$H_{dip} = \frac{\mu_o \beta^2}{4\pi r^3}\left((\mathbf{g}_A \vec{S}_A)(\mathbf{g}_B \vec{S}_B) - 3\frac{(\vec{r}\,\mathbf{g}_A \vec{S}_A)(\vec{r}\,\mathbf{g}_B \vec{S}_B)}{r^2}\right) \tag{4}$$

where $\mathbf{g}_A$ and $\mathbf{g}_B$ are the **g** tensors of the two centers A and B, **J** is the exchange coupling tensor, and r is the intercenter distance; the program calculates the positions and the transition probabilities of the resonance lines. The line widths are considered to arise essentially from strain effects, which are treated by a procedure recently described (Bertrand et al., 1994). In this procedure, all the parameters describing the magnetic characteristics and the geometrical arrangement of the system are considered as random variables characterized by their mean values and their standard deviations. In practice, good simulations were obtained by assuming that a limited number of parameters were distributed. The **J** tensor was assumed to be isotropic. Numerical simulations were performed on an IBM 3090 computer with typical CPU calculation time of about 40 s.

Relaxation Time Measurements. The measurement of T_1 and T_2 by electron spin echo methods was carried out on a Bruker ESP 380 spectrometer fitted with an Oxford Instruments CF935 cryostat. The spin−spin relaxation time T_2 was determined by using a two-pulse sequence ($\pi/2-\tau-\pi$) and by fitting the average of the modulated electron spin echo envelope to a monoexponential decay. The spin−lattice relaxation time T_1 was obtained by saturation−recovery experiments employing a long-duration saturation pulse followed, after a variable time interval t, by a two-pulse sequence ($\pi/2-\tau-\pi$), with τ = 112 ns, to probe the magnetization recovery. The widths of the $\pi/2$ and π pulses were 16 and 32 ns, respectively, and the repetition time of the sequence was 1 ms.

The relaxation times T_1 and T_2 of the Ni center were also measured by continuous-wave power-saturation experiments. Saturated spectra were assumed to be the convolution product between the unsaturated spectrum and saturated lorentzian spin-packets (Castner, 1959). Saturation curves, giving the variations of the signal amplitude as a function of the microwave magnetic field B_1, were numerically computed for different half-widths ΔB_p of the spin-packets. The two parameters ΔB_p and $B_{1/2}$, where $B_{1/2}$ is the magnetic field at half-saturation, were derived by comparison of the experimental data with these calculated saturation curves. The relaxation rates were then deduced from

$$\frac{1}{T_2} = \frac{g\beta}{\hbar}\Delta B_p \qquad \frac{1}{T_1} = \frac{g\beta (B_{1/2})^2}{\hbar \Delta B_p} \tag{5}$$

Analysis of the Relaxation Times. When a slowly relaxing paramagnetic center is magnetically coupled to a fast one, it undergoes an enhancement of its spin−lattice and spin−spin relaxation rates, which are given respectively by (Hirsh et al., 1992; Goodman & Leigh, 1985)

$$k_1 = k_{1s} + k_{1ex} + k_{1dip} \tag{6}$$

$$k_2 = k_{2s} + k_{2ex} + k_{2dip} \tag{7}$$

where $k_{is} = 1/T_{is}$ (i = 1, 2) are the intrinsic relaxation rates of the slowly relaxing center and k_{iex} and k_{idip} (i = 1, 2) represent the enhancement of the relaxation rates due to the exchange and dipolar couplings between the two centers, respectively. In the case of a fast-relaxing center with spin $S = {}^1/_2$, the expressions for k_{1ex} and k_{2ex} given by Hirsch et al. (1992) lead to

$$k_{1ex} = 2J^2 \frac{T_{2f}}{1 + \omega^2 T_{2f}^2\left(1 - \frac{g_f}{g_s}\right)^2} \tag{8}$$

$$k_{2ex} = J^2\left(T_{1f} + \frac{T_{2f}}{1 + \omega^2 T_{2f}^2\left(1 - \frac{g_f}{g_s}\right)^2}\right) \tag{9}$$

where J is the exchange parameter defined in eq 3, T_{1f} and T_{2f} are the spin−lattice and spin−spin relaxation times of the fast-relaxing center, g_s and g_f are the effective g-values of the slow- and fast-relaxing centers, respectively, and ω is the microwave angular frequency used in the EPR experiment. The whole expressions of k_{1dip} and k_{2dip} contain several terms involving the intercenter distance r and the angle γ between the magnetic field and the intercenter vector (Hirsh et al., 1992; Goodman & Leigh, 1985). Owing to the values of T_{1f} and T_{2f} that we measured (see below), the dominant terms in those expressions are expected to be

$$k_{1dip} = \left(\frac{\mu_0}{4\pi}\right)^2 \frac{\beta^4 g_f^2 g_s^2}{8\hbar^2 r^6}(1 - 3\cos^2\gamma)^2 A \tag{10}$$

$$A = \frac{T_{2f}}{1 + \omega^2 T_{2f}^2\left(1 - \frac{g_f}{g_s}\right)^2}$$

$$k_{2dip} = \left(\frac{\mu_0}{4\pi}\right)^2 \frac{\beta^4 g_f^2 g_s^2}{4\hbar^2 r^6}(1 - 3\cos^2\gamma)^2 T_{1f} \tag{11}$$

Equations 8−11 are valid within the Redfield limit, which

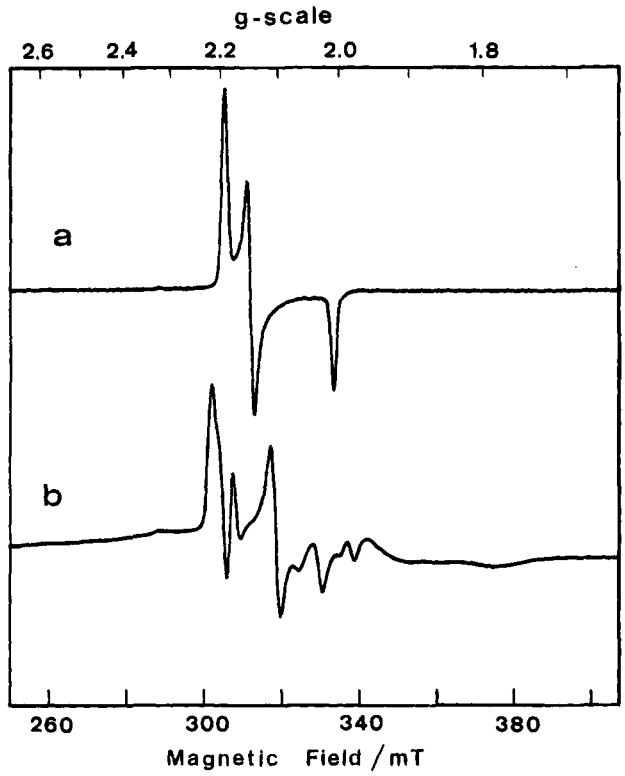

FIGURE 1: X-band EPR spectra of *D. gigas* hydrogenase Ni−C state. (a) Unsplit Ni−C signal given by a sample poised at −354 mV. (b) Split Ni−C signal given by a sample poised at −376 mV. Experimental conditions: temperature, 4.2 K; microwave frequency, 9.378 GHz; microwave power, 0.01 mW (a) or 1 mW (b); modulation frequency, 100 kHz; modulation amplitude, 1 mT.

requires that

$$T_{1f} \text{ and } T_{2f} \ll T_{1s} \text{ for eqs 8 and 10}$$

$$T_{1f} \text{ and } T_{2f} \ll T_{2s} \text{ for eqs 9 and 11}$$

In our analysis of the magnetic properties of the active state of *D. gigas* hydrogenase, the Ni−C center and the [4Fe-4S]$^{1+}$ clusters are considered as the slow- and fast-relaxing species, respectively.

RESULTS

Numerical Simulation of EPR Interaction Spectra. The redox behavior of *D. gigas* hydrogenase has been already studied in detail by EPR and Mössbauer spectroscopies (Cammack et al., 1987; Teixeira et al., 1989). During the reduction of the enzyme by hydrogen gas, the Ni−C signal intensity (Figure 1a) shows a bell-shaped curve characterized by midpoint potentials E_{m7} of about −270 and −390 mV for its appearance and disappearance, respectively. The reduction of the [4Fe-4S] clusters occurs with an E_{m7} value of about −350 mV and gives rise to a broad, fast-relaxing EPR signal. At low temperature (<10 K), the magnetic interactions between the reduced [4Fe-4S]$^{1+}$ clusters and the Ni center change the Ni−C signal into a complex EPR signal with prominent features at $g = 2.21$ and 2.10 (Figure 1b). In the following, this signal will be termed the "split Ni−C signal". All these E_m values are pH-dependent, varying by approximately −120 mV/pH unit for the appearance of the Ni−C signal and by −60 mV/pH unit for both the disappearance of the Ni−C signal and the appearance of the broad [4Fe-4S]$^{1+}$ signal. Consequently, the Ni−C species can be detected over a wider range of potential but reaches a higher concentration at more acidic pH. We have taken advantage of this property by preparing the samples at pH 6.5, so as to obtain the pure and intense unsplit and split Ni−C signals required for our detailed spectroscopic studies.

The comparison of the unsplit and split Ni−C signals (Figure 1) shows clearly that the $g_X = 2.192$ and $g_Y = 2.145$ features of the former are split into two components at $g = 2.217$ and 2.177 and $g = 2.195$ and 2.104, respectively, in the latter. This simple splitting pattern suggests that the Ni−C center is magnetically coupled to a single paramagnetic species. Since the split Ni−C signal is only observed when the [4Fe-4S] clusters are chemically reduced, this paramagnetic species is necessarily a [4Fe-4S]$^{1+}$ center. The EPR spectrum given by two magnetically interacting species is known to be strongly dependent on the relative arrangement of the two interacting paramagnets (Guigliarelli et al., 1993; Bertrand et al., 1994), so that the analysis of the split Ni−C signal appears as an attractive way to determine the structural organization of the Ni site and of the closest [4Fe-4S]$^{1+}$ center.

The input data of the spectral simulation program implemented to perform this analysis are the principal values of the $\mathbf{g}_{Ni}$ and $\mathbf{g}_{4Fe}$ tensors, the three Euler angles (a, b, c), which define the orientation of the magnetic axes of the Ni center with respect to those of the [4Fe-4S]$^{1+}$ cluster, the exchange coupling constant J, and the spherical polar coordinates (r, θ, ϕ), which determine the position of the Ni center with respect to the [4Fe-4S] cluster (Guigliarelli et al., 1993). Among these parameters, only the principal values of the $\mathbf{g}_{Ni}$ tensor could be experimentally obtained by simulating the unsplit Ni−C signal (Figure 2a). By contrast, the broad and structureless EPR signal associated with the reduction of the [4Fe-4S] clusters (Figure 1b) arises very likely from the magnetic interactions between these clusters and the reduced [3Fe-4S]^0 center (Teixeira et al., 1989), so that the principal values of the $\mathbf{g}_{4Fe}$ tensor cannot be experimentally determined. The unknown parameters used in the simulation are then too numerous to allow a systematic search in the parameter space, so that it is essential to guide their adjustment by an understanding of the main features of the interaction spectrum (Guillaussier, 1991).

As the starting point of the parameter adjustment, we first consider the effect of the exchange interactions. Schematically, for a given orientation of the magnetic field $\vec{B}$, the exchange interactions between two anisotropic paramagnets can give rise to two limit situations: (i) When $|2J| \ll |\Delta g \beta B|$, where Δg represents the difference between the effective g-values of the two centers, the first-order effect of the exchange interaction splits the line given by each center into two components of equal amplitudes separated by $J/g\beta$ in the field units. (ii) When $|2J| \simeq |\Delta g \beta B|$, second-order effects must be taken into account, so that the central lines of the splitting pattern collapse on their mean position, and the amplitude of the outer lines decreases strongly. We first consider the simple physical case where the magnetic axes of the two centers are parallel, and we assume that the g-values of the [4Fe-4S]$^{1+}$ cluster are similar to those measured for [4Fe-4S]$^{1+}$ centers in ferredoxins. For instance, we use in a first step the set $g_{z(4Fe)} = 2.075$, $g_{y(4Fe)} = 1.95$, and $g_{x(4Fe)} = 1.85$. The examination of the split

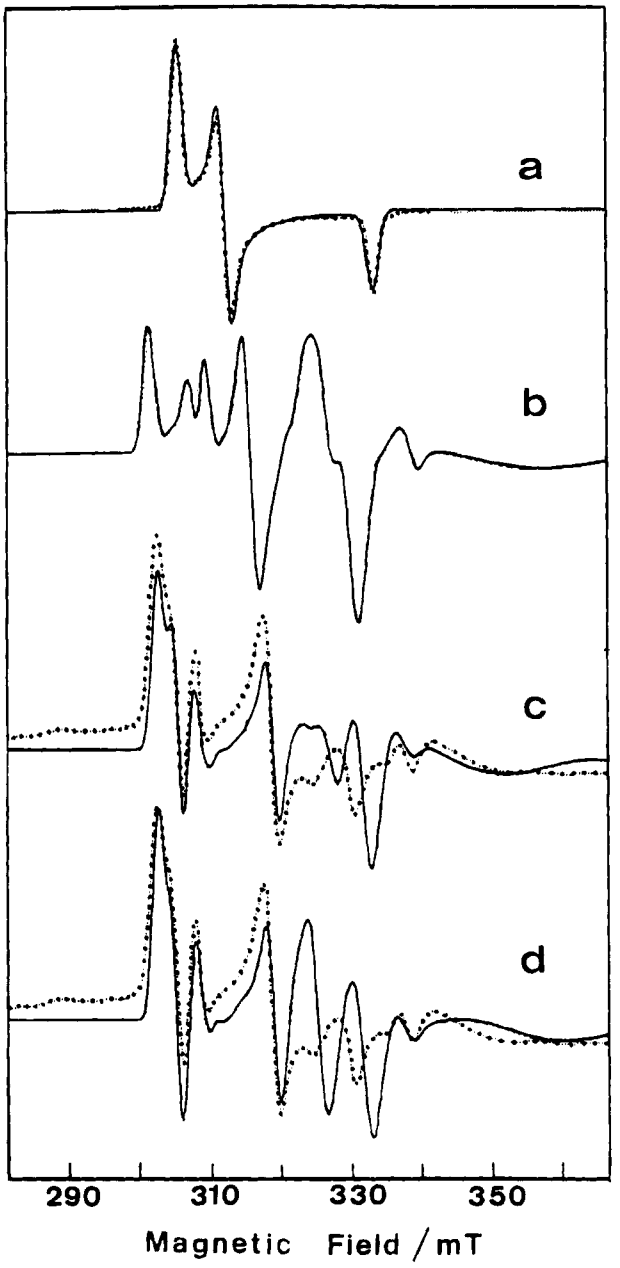

FIGURE 2: Parameter adjustment in the numerical simulation procedure of the split Ni−C signal recorded at X-band. Solid lines, simulated spectra. (a) Unsplit Ni−C signal: $J = 0$, $r = \infty$. (b) $|J| = 40 \times 10^{-4}$ cm^{-1}, $(a, b, c) = (90°, 90°, 90°)$, $r = \infty$. (c) $J = 40 \times 10^{-4}$ cm^{-1}, $r = 0.85$ nm, $\Theta = 90°$, $\phi = 0°$, $(a, b, c) = (0°, 90°, 90°)$. (d) Same parameters as for (c) except $(a, b, c) = (90°, 90°, 90°)$. Other parameters used in the simulations are given in Table 1 except $g_{(4Fe)} = 2.075, 1.95, 1.85$. Dotted lines, experimental spectra with the same conditions as for Figure 1a (a) or Figure 1b (c and d).

Ni−C signal (Figure 1b) indicates that the low-field part of the spectrum ($g > 2.10$) arises from the first-order effect of the exchange interaction, whereas the high-field part is due to second-order effects. Owing to the g-values of Ni−C and [4Fe-4S]$^{1+}$ centers, such a splitting pattern is expected only when the magnetic axis X_{Ni} is parallel either to Z_{4Fe} or to Y_{4Fe}. Two geometrical configurations correspond to each possibility, the Y_{Ni} axis being parallel either to Y_{4Fe} or to X_{4Fe} in the former, and to X_{4Fe} or Z_{4Fe} in the latter. These four relative orientations of the $\mathbf{g}_{Ni}$ and $\mathbf{g}_{4Fe}$ tensors are described respectively by the four sets of Euler angles, (90°, 90°, 90°), (0°, 90°, 90°), (90°, 0°, 0°), and (90°, 90°, 0°). The average of the splittings observed for the $g_{Z(Ni)}$ and $g_{Y(Ni)}$ peaks of the split Ni−C signal can be evaluated at about 8 mT. EPR spectra were calculated by considering an exchange interaction $|2J/g\beta|$ of this magnitude for the four sets of Euler angles defined above. The four spectra were very similar, displaying well-defined splittings at low field ($g > 2.10$) and second-order-type features at high field (Figure 2b). As expected, the splittings of the $g_{Z(Ni)}$ and $g_{Y(Ni)}$ peaks are equal on these calculated spectra, so that the anisotropy observed on the experimental spectrum can be reproduced only by introducing the dipolar interactions.

Schematically, in a powder spectrum, the dipolar contribution to the splitting of the g_u peak ($\vec{u} = \vec{x}, \vec{y}, \vec{z}$) varies as $(1 - 3\cos^2 \gamma_u)$, γ_u being the angle between the magnetic axis $\vec{u}$ and the interspin vector $\vec{r}$. In order to slightly decrease the splitting of the $g_{Z(Ni)}$ peak and to increase more strongly that of the $g_{Y(Ni)}$ peak, the angles $\gamma_{Z(Ni)}$ and $\gamma_{Y(Ni)}$ must be close to 90° and 0°, respectively. This corresponds to the intercenter vector $\vec{r}$ lying along the Y_{Ni} axis. By use of this simple configuration, the improvement of the simulation required additional constraints on the sign of J and on the distance r, leading to a rough estimation of this parameter in the range 8−9 Å. Remarkably enough, in these conditions, the four sets of Euler angles previously defined gave correct simulations of the low-field part of the split Ni−C signal, the different peaks being well positioned and their relative amplitude correctly reproduced (Figure 2c,d). The parameter space was then extensively explored around each of these four simple geometrical arrangements, in order to improve the simulation of the high-field part of the signal ($g < 2.10$). This improvement was not possible by keeping the X_{Ni} axis close to Y_{4Fe}, which ruled out the corresponding configurations. Finally, the last step of the parameter refinement was performed by simulating the split Ni−C signal recorded at three different microwave frequencies, at X-band, Q-band, and S-band (Figure 3).

As expected for an interaction spectrum, the shape of the split Ni−C signal is strongly frequency-dependent, and at high frequency (Q-band), the condition $|2J| \ll \Delta g\beta B$ becomes valid even in the high-field part of the spectrum, leading to a well-defined splitting of the $g_{Y(Ni)}$ peak (Figure 3b). In contrast, at low frequency (S-band), the second-order effects of the exchange interaction are likely to contribute to a large part of the spectrum, which precludes any simple interpretation of the experimental signal (Figure 3c). The standard deviations of the Ni−C g-values used to simulate the line width of the unsplit Ni−C signal depend on the frequency (Table 1), which indicates that hyperfine interactions contribute significantly to the broadening of the Ni−C spectra. However, the broadening of the interaction spectra could be accounted for in our simulations by resorting to a simple g-strain procedure. At X-band, the shape of the high-field part of the calculated spectrum was very sensitive to the $g_{Z(4Fe)}$ and $g_{Y(4Fe)}$ values. Correct simulations of this region required a rather high g_Z value for a [4Fe-4S]$^{1+}$ cluster (Table 1), close to that measured for center X in cyanobacterial photosystem I (Guigliarelli et al., 1993). Moreover, large standard deviations of the g_{4Fe} values were used to account for the large broadening of the Fe−S signal. This broadening, which is not usual for a [4Fe-4S]$^{1+}$ signal, arises probably from the magnetic interactions between this center and the other Fe−S clusters. The best simulations of

Table 1: Parameter Values Leading to the Best Numerical Simulations of the Split Ni−C EPR Signal at X-Band, Q-Band, and S-Band[a]

	$g_x(\sigma_x)$		$g_y(\sigma_y)$		$g_z(\sigma_z)$	
Ni center	2.010	$(5.5 \times 10^{-3})^b$	2.146	$(5.7 \times 10^{-3})^b$	2.194	$(5.9 \times 10^{-3})^b$
		$(1.7 \times 10^{-3})^c$		$(3.5 \times 10^{-3})^c$		$(2.8 \times 10^{-3})^c$
		$(16 \times 10^{-3})^d$		$(17 \times 10^{-3})^d$		$(17.7 \times 10^{-3})^d$
$[4Fe\text{-}4S]^{1+}$ center	1.860	(30×10^{-3})	1.915	(30×10^{-3})	2.137	(40×10^{-3})
J	40×10^{-4} cm^{-1}		(r, θ, ϕ)		(0.86 nm, 85°, 60°)	
(a, b, c)	(56°, 72°, 105°)					

[a] The accuracy of the parameters is about 5° for angles, 0.05 nm for the distance r, and 0.5×10^{-3} cm^{-1} for the exchange parameter J. [b] Standard deviation characterizing the g-strain at X-band. [c] Standard deviation at Q-band. [d] Standard deviation at S-band.

the split Ni−C signal obtained by using the same set of parameters (Table 1) at the three frequencies are given in Figure 3. At X-band and Q-band, the positions of the lines and their relative amplitudes are fairly well reproduced (Figure 3a,b). At S-band, the agreement between the calculated and experimental spectra is slightly less satisfactory (Figure 3c). This is probably due to the relatively simplified description of the broadening processes, which takes into account neither the statistical distribution of the structural parameters nor that of the exchange coupling constant (Guigliarelli et al., 1993).

Analysis of the Ni−C Relaxation Times. At low temperature (4.2 K), the split and unsplit Ni−C signals exhibit very different power saturation properties: the unsplit Ni−C signal begins to saturate for microwave powers higher than 10 μW, whereas the split Ni−C signal remains unsaturated up to 1 mW. These different saturation behaviors clearly indicate that the relaxation of the Ni−C species is strongly enhanced by the magnetic coupling with the fast-relaxing Fe−S clusters (Van Der Zwaan et al., 1987; Teixeira et al., 1989). Continuous-wave saturation experiments were performed at 4.2 K, on the derivativelike peaks at $g = 2.10$ and 2.14, for the split and unsplit Ni−C signals, respectively (Figure 4). Fitting the experimental data obtained for the unsplit Ni−C (Figure 4) to computed saturation curves gave the half-width of the spin-packets $\Delta B_P = 0.035$ mT and the microwave power at half-saturation $P_{1/2} = 90$ μW, which led to the intrinsic relaxation times of the Ni−C species, $T^{\circ}_{2(Ni)} = 0.15$ μs and $T^{\circ}_{1(Ni)} = 180$ μs. Even at the maximum available power, the saturation of the split Ni−C signal was not sufficient to determine unambiguously ΔB_P and $P_{1/2}$ (Figure 4). However, by assuming that ΔB_P is the same for the split and unsplit Ni−C signals, the value $P_{1/2} = 3$ mW was obtained, giving the estimated values $T_{2(Ni)} = 0.15$ μs and $T_{1(Ni)} = 7$ μs for the Ni−C center when magnetically coupled to the $[4Fe\text{-}4S]^{1+}$ cluster (Table 2).

In order to determine the relaxation times of the Fe−S cluster, which are too short to be obtained by continuous saturation methods, spin−echo experiments were carried out at liquid helium temperature. The relaxation rates of the $[4Fe\text{-}4S]^{1+}$ centers were measured at $g = 2.26$ and 1.91, in a region of the coupled Ni−C spectrum where the Ni center does not contribute, and gave the values $T_{2(4Fe)} = 0.2$ μs and $T_{1(4Fe)} = 5$ μs (Figure 5a). We have also performed spin−echo experiments at $g = 2.10$, which corresponds to the maximum of the Ni−C absorption spectrum. The superposition of signals arising from the Ni and $[4Fe\text{-}4S]^{1+}$ centers precluded an accurate determination of the Ni−C species relaxation properties. However, the spin−spin relaxation time $T_{2(Ni)}$ could be estimated at about 0.3 μs, a value close to that of the $[4Fe\text{-}4S]^{1+}$ cluster. In addition, the magnetization recovery at $g = 2.10$ showed non-single-exponential kinetics, reflecting a distribution of the $T_{1(Ni)}$ values, ranging from about 5 μs to about 50 μs (Figure 5b). For the unsplit Ni−C signal, spin−echo measurements were performed at $g = 2.14$, which corresponds to the maximum of the EPR absorption spectrum, and gave the values $T^{\circ}_{2(Ni)} = 0.3$ μs and $T^{\circ}_{1(Ni)} = 250$ μs. Thus, within experimental error, the Ni−C relaxation times obtained by pulsed EPR experiments are consistent with those measured by the continuous-wave saturation method (Table 2).

The comparison of these different relaxation times shows that at 4.2 K the magnetic interactions between the Ni−C and the $[4Fe\text{-}4S]^{1+}$ centers enhance essentially the spin−lattice relaxation of the Ni−C center. This is due to the fact that, at this temperature, the intrinsic spin−spin relaxation time $T^{\circ}_{2(Ni)}$ of the Ni−C species is not much longer than $T_{1(4Fe)}$ and $T_{2(4Fe)}$, so that it is not significantly affected by the magnetic coupling. In this case, eqs 9 and 11 are no longer valid and should be replaced by the following equation (Goodman & Leigh, 1985):

$$\frac{1}{T_{2(Ni)}} = \frac{1}{T^{\circ}_{2(Ni)}} + \frac{1}{2T_{1(4Fe)}} \qquad (12)$$

which is not dependent on the relative arrangement of the two centers. This equation is satisfied by our experimental data, within experimental error. In contrast, $T^{\circ}_{1(Ni)}$ is much longer than the Fe−S relaxation times and eqs 8 and 10 apply. The spin−lattice relaxation of the split Ni−C signal was measured at $g = 2.10$, on a feature arising from the splitting of $g_{y(Ni)}$ peak. The resonance lines contributing to this part of the spectrum originate from hydrogenase molecules whose orientation is such that the effective $g_{(Ni)}$ value is equal to $g_{y(Ni)}$. Within this class of molecules, the effective $g_{(4Fe)}$ value varies, leading to a broad distribution of the factor $(1 - g_{4Fe}/g_{Ni})^2$ involved in the expression of k_{1ex} and k_{1dip} (eqs 8 and 10). This explains the non-single-exponential relaxation kinetics observed experimentally. Despite this difficulty, we have attempted to verify whether the low-temperature relaxation data are consistent with the relative arrangement of the Ni and [4Fe-4S] centers deduced from the spectral simulations (Table 1). We first observe that, according to eqs 8 and 10, the ratio k_{1dip}/k_{1ex} is independent of this factor but depends strongly on the parameters J and r:

$$\frac{k_{1dip}}{k_{1ex}} = \left(\frac{\mu_o}{4\pi}\right)^2 \frac{\beta^4 g_{Ni}^2 g_{4Fe}^2}{6\hbar^2 J^2 r^6} (1 - 3\cos^2\gamma)^2 \qquad (13)$$

By using the average value of the angular factor, $\langle(1 - 3\cos^2\gamma)^2\rangle = {}^4/_5$, and the values of J and r given in Table 1,

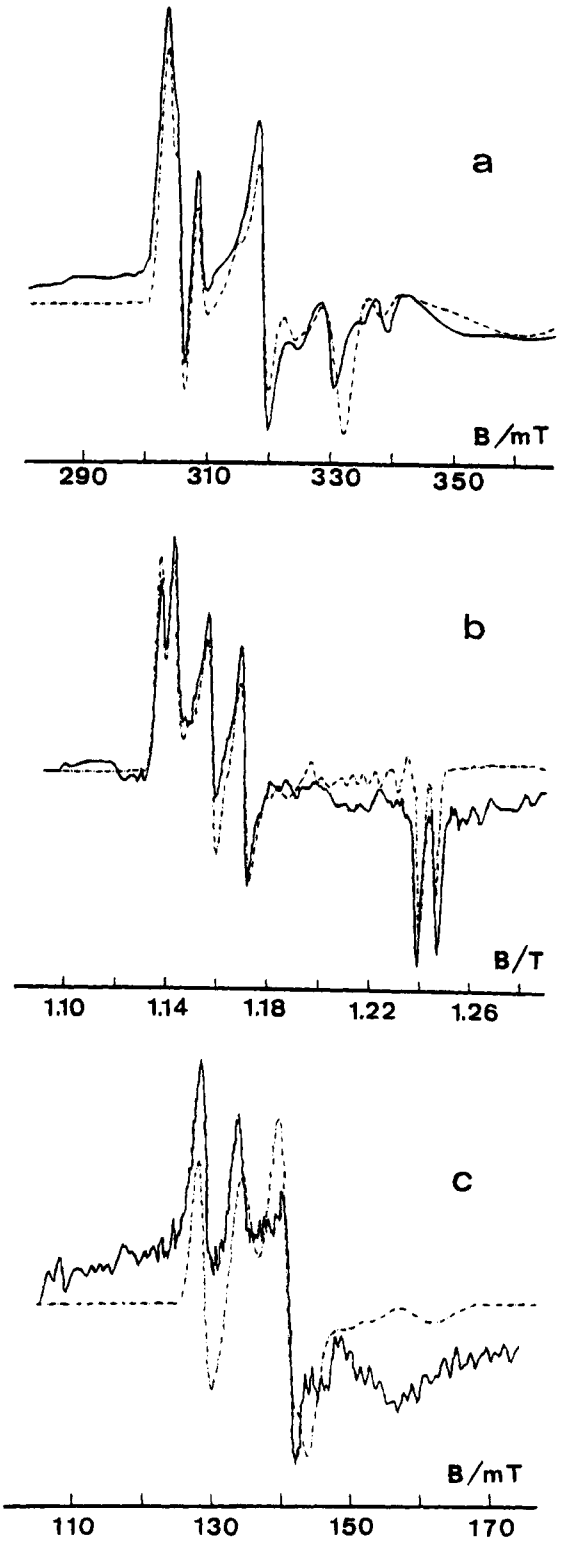

FIGURE 3: X-band, Q-band, and S-band EPR spectra given by *D. gigas* hydrogenase in the split Ni−C state. Solid lines, experimental spectra with the following conditions: temperature, 4.2 K (a), 7 K (b), or 5.5 K (c); microwave frequency, 9.378 GHz (a), 34.95 GHz (b), or 4.051 GHz (c); microwave power, 1 mW (a), 5 mW (b), or 2 mW (c); modulation frequency, 100 kHz (a and c) or 1 kHz (b); modulation amplitude, 1 mT (a, b) or 0.5 mT (c). Dotted lines, numerical simulations obtained with the parameters listed in Table 1.

we found that this ratio is close to unity. This shows that the dipolar and exchange interactions contribute equally to the enhancement of the spin−lattice relaxation of Ni. Now,

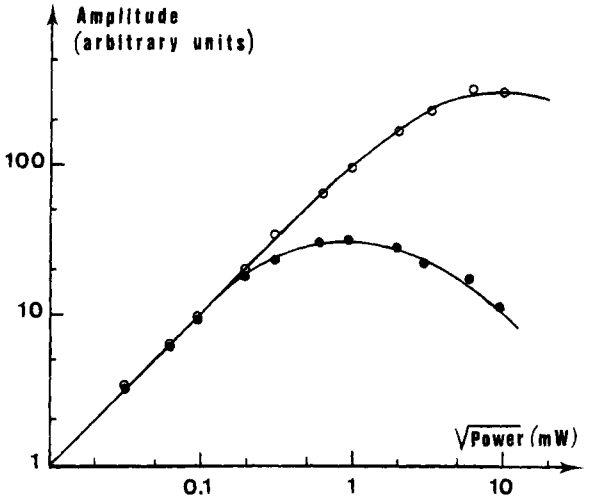

FIGURE 4: Continuous microwave power saturation of the Ni−C signals. The peak-to-peak amplitude was measured at $g = 2.14$ (●) for the unsplit Ni−C signal and at $g = 2.10$ (○) for the split Ni−C signal. Other conditions are as in Figure 1. The solid lines are saturation curves calculated for $\Delta B_P = 0.035$ mT and $P_{1/2} = 90$ μW and 3 mW for the unsplit and split Ni−C signals, respectively.

Table 2: Relaxation Time Measurements at 4.2 K of the Ni and (4Fe−4S) Centers in the Ni−C State of the *D. gigas* Hydrogenase

	T_2 (μs)		T_1 (μs)	
	power saturation	pulsed EPR	power saturation	pulsed EPR
unsplit Ni−C signal ($g = 2.14$)	0.15	0.3	180	250
split Ni−C signal ($g = 2.10$)	0.15	0.3	7	5−50
$(4Fe-4S)^{1+}$ signal ($g = 1.91$)		0.2		5

if we consider the relative arrangement of the Ni and [4Fe-4S] centers deduced from the spectral simulations (Table 1), the angular factor $(1 - 3\cos^2\gamma)^2$ is equal to 4 when the magnetic field is parallel to the $g_{y(Ni)}$ axis. For this particular orientation, eqs 8 and 10 give

$$k_{1ex} = 4.2 \times 10^3\ s^{-1} \quad \text{and} \quad k_{1dip} = 23 \times 10^3\ s^{-1}$$

by using the value $T_{2(4Fe)} = 0.2$ μs (Table 2). By taking $T^{\circ}_{1(Ni)} = 200$ μs, these values led to the estimation $T_{1(Ni)} = 30$ μs, in good agreement with spin−echo measurements (Table 2).

Between 8 and 12 K, the split lines of the split Ni−C signal collapse progressively (Figure 6a,b), leading at higher temperature to an EPR signal which looks like the unsplit Ni−C signal (Figure 6c,d). This collapse reflects the increase of the $[4Fe-4S]^{1+}$ spin−lattice relaxation rate, whose magnitude becomes equivalent to that of the static splittings expressed in frequency units (Goodman & Leigh, 1985). Owing to the anisotropy of the splittings, the collapse of the different lines does not occur at the same temperature, which gives complicated spectral shapes between 8 and 12 K (Figure 6b). Above 12 K, the presence of magnetic interaction is only manifested by a broadening of the Ni−C signal, which decreases progressively when the temperature increases (Figure 6c,d) and leads to an EPR signal identical to the unsplit Ni−C signal (Figure 1a) for temperatures higher than 50 K. Moreover, the coupled and uncoupled Ni−C signals exhibit different saturation properties, a phenomenon that is observable up to 100 K. At 15 K, for

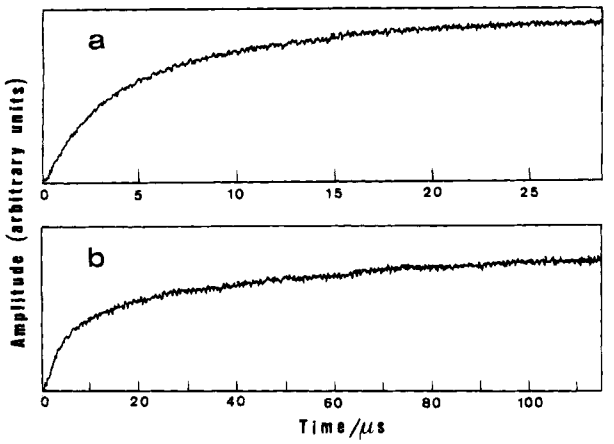

FIGURE 5: Saturation–recovery transients observed at 4.2 K for the split Ni–C signal at $g = 1.91$ (a) and at $g = 2.10$ (b). The traces are arbitrarily scaled vertically.

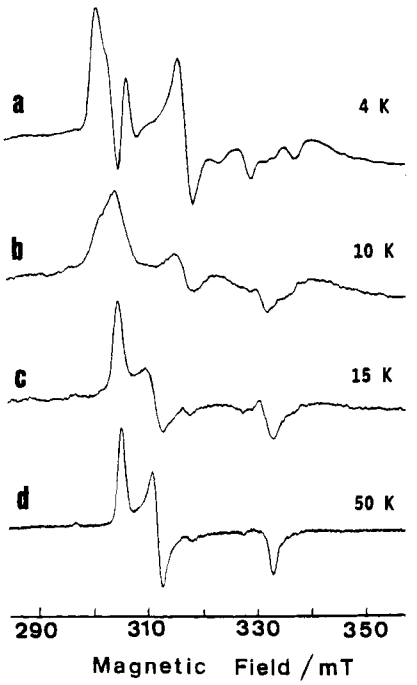

FIGURE 6: Temperature dependence of the split Ni–C signal. The EPR spectra were recorded with a microwave power of 1 mW at 4 K and 10 mW at other temperatures. Except for the modulation amplitude (0.5 mT), other conditions were as for Figure 1.

instance, the uncoupled Ni–C signal begins to saturate at 1 mW, whereas the coupled Ni–C signal remains unsaturated at 100 mW. In the temperature range 4.2–30 K, spin–echo measurements showed that $T^{\circ}_{1(Ni)}$ varies as T^{-1}, from 250 to 30 μs. In the same range $T^{\circ}_{2(Ni)}$ was temperature-independent and equal to 0.3 μs. Above 12 K, T_1 of the coupled Ni, $T_{1(Ni)}$, was too short to be measured by pulsed EPR experiments, which ruled out any quantitative analysis of the Ni–C spin–lattice relaxation. In contrast, the broadening of the coupled Ni–C signal is directly related to the shortening of $T_{2(Ni)}$, which provides a useful method to analyze the spin–spin relaxation quantitatively.

The unsplit Ni–C signal results from the convolution product between the spectrum envelope and a Lorentzian spin-packet whose half-width is proportional to $1/T^{\circ}_{2(Ni)}$ (eq 5). In the same way, above 12 K, the coupled Ni–C signal can be considered as the convolution product between the

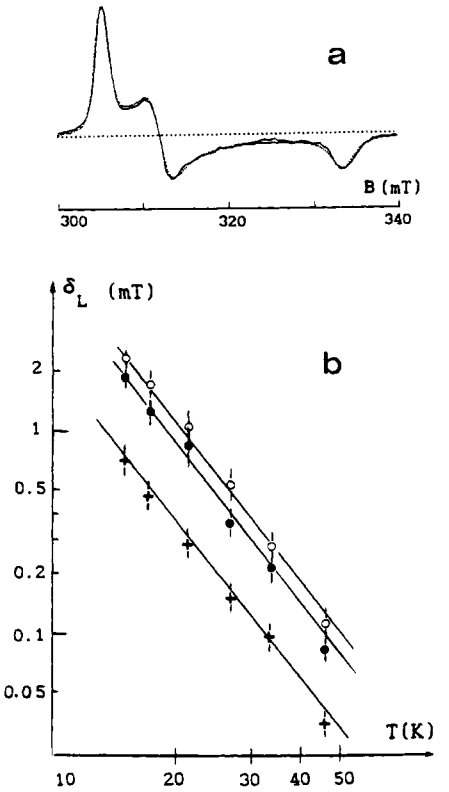

FIGURE 7: Study of the broadening of the coupled Ni–C EPR signal. (a) Simulation of the broadening. Solid line, experimental spectrum of the coupled Ni–C center at 21 K; dotted lines, calculated spectra resulting from the convolution product of the unsplit Ni–C signal given in Figure 1a, with a Lorentzian line whose half-widths along the three magnetic axes of the Ni–C center are equal to $\delta_X = 1.1$ mT, $\delta_Y = 0.9$ mT, and $\delta_Z = 0.25$ mT, respectively. (b) Temperature dependence of the half-width of the Lorentzian line. (○) δ_X, (●) δ_Y, (+) δ_Z.

same spectrum envelope and Lorentzian spin-packets whose half-width is proportional to $1/T_{2(Ni)}$. Therefore, this signal can be simulated by convoluting numerically the uncoupled Ni–C signal with a Lortentzian line whose half-width δ_L is proportional to $[(1/T_{2(Ni)}) - (1/T^{\circ}_{2(Ni)})] = k_{2ex} + k_{2dip}$ (eq 7). To account for the anisotropy of the broadening, different values of δ_L were considered for each magnetic axis of the Ni–C center (Figure 7a). The broadening of the coupled Ni–C signal was simulated in this way between 13 and 50 K, and the values of δ_L are plotted as a function of temperature in Figure 7b. By comparison with the Fe–S signal recorded at 4.2 K, the relaxation broadening of the Fe–S signal at 15 K was estimated at about 5 mT in the $g = 1.95$ region, which leads to $T_{1(4Fe)}$ and $T_{2(4Fe)}$ values of about 10^{-9} s. These values are much shorter than $T_{2(Ni)}$, so that eqs 9 and 11 are valid. In these conditions, the second term of eq 9 is negligible, and this equation becomes

$$k_{2ex} = J^2 T_{1(4Fe)} \tag{14}$$

From eqs 11 and 14, it appears that the spin–spin relaxation enhancement of the Ni–C center, $(1/T_{2(Ni)}) - (1/T^{\circ}_{2(Ni)})$, is then directly proportional to $T_{1(4Fe)}$, so that the temperature dependence of δ_L represents that of $T_{1(4Fe)}$ (Figure 7b). When the temperature increases, the shortening of $T_{1(4Fe)}$ is then responsible for the unusual increase of $T_{2(Ni)}$. By using the structural parameters deduced from the simulation of the split Ni–C signal (Table 1), the effective g_{4Fe} values and the γ

angle involved in eq 11 were calculated for each magnetic direction of the Ni−C center. Using these values together with eqs 5, 11, and 14, we obtain at 15 K $\delta_Z = 0.5$ mT, $\delta_X = 0.55$ mT, and $\delta_Y = 0.8$ mT. The magnitude of these calculated broadenings is in agreement with the experimental data (Figure 7b), but not their anisotropy, suggesting that $T_{1(4Fe)}$ is also anisotropic. The anisotropy of the intrinsic spin−lattice relaxation time has already been observed for magnetically isolated Fe−S clusters (Hagen & Albracht, 1982). In the case of the [4Fe-4S]$^{1+}$ of *D. gigas* hydrogenase, an additional cause of anisotropy arises from the magnetic interactions between the [4Fe-4S]$^{1+}$ clusters and the reduced [3Fe-4S]^{o} center.

DISCUSSION

The knowledge of the relative organization of the Ni site and of the Fe−S centers is essential for understanding the mechanism by which electrons are transferred to and from the catalytic site of NiFe hydrogenases. To address this question, we have undertaken a study of the spin−spin interactions observed by EPR spectroscopy between the Ni and Fe−S centers in the Ni−C state of the *D. gigas* enzyme. The possibility of preparing the active form of this hydrogenase in two well-defined redox states, the [4Fe-4S] clusters being either oxidized or reduced, enabled us to perform for the first time a detailed analysis of both the static and dynamic effects of magnetic interactions between paramagnetic centers in a biological system.

The static effect is manifested by the appearance of a complex nickel EPR signal at low temperature, the split Ni−C signal. This signal was analyzed by a numerical simulation procedure based on a general treatment of the dipolar and exchange interactions between closely spaced paramagnets. A first-order analysis of the main features of the interaction spectrum showed that only one [4Fe-4S]$^{1+}$ cluster is significantly coupled to the Ni−C center and led to a limited number of possible schematic arrangements of the two centers. This number of possibilities was subsequently restricted by improving the simulation of the split Ni−C signal, which finally led to a detailed description of the structural organization of the two centers (Table 1). Our ability to simulate this signal recorded at three different microwave frequencies with the same set of structural parameters provides a strong support for the uniqueness of these parameters and for the correctness of our spectral analysis.

In addition, the magnetic characteristics of the [4Fe-4S]$^{1+}$ cluster coupled to the Ni site, which are hidden by the spin-coupling with the other Fe−S centers, could be deduced from this analysis. The **g**-tensor of this cluster is markedly more anisotropic than those of the [4Fe-4S]$^{1+}$ from ferredoxins (Table 1), with broader resonance lines, and a very fast spin−lattice relaxation time (Table 2). These properties resemble those of center X of photosystem I (Bertrand et al., 1988; Guigliarelli et al., 1993), which is a [4Fe-4S] cluster in a bridging position between two polypeptides (Golbeck et al., 1987), and those of the $S = {}^1/_2$ spin state of the [4Fe-4S]$^{1+}$ center in the *Pyrococcus furiosus* ferredoxin (Conover et al., 1990), which is coordinated by a non-cysteine ligand. In both cases, these magnetic properties are likely related to the unusual coordination of the metal center. In the small subunit of the *D. gigas* hydrogenase, which is considered as carrying the Fe−S clusters, only 10 conserved Cys residues have been reported (Voordouw, 1992). These residues are not sufficient to coordinate the three Fe−S centers of the enzyme, and are not arranged in the typical motif found in 4Fe ferredoxins. A coordination by an unusual cysteine pattern could then explain the peculiar magnetic properties of the [4Fe-4S] cluster closest to the Ni site.

The nature of the dynamic effects of the spin−spin interactions in the Ni−C state is determined by the relaxation properties of the [4Fe-4S]$^{1+}$ cluster. At low temperature, the intrinsic spin−spin relaxation times T_2 of the Ni and [4Fe-4S] centers are not very different, and only the Ni spin−lattice relaxation time T_1 is significantly shortened by the interaction (Table 2). For temperatures higher than 8 K, the shortening of $T_{1(4Fe)}$ causes the disappearance of the static effect of the spin-coupling, while the dynamic effects are manifested by the power saturation behavior and the broadening of the Ni−C signal. The spin−spin relaxation enhancement of the Ni center was deduced from this broadening and showed a temperature dependence inversely proportional to that of $T_{1(4Fe)}$. All these relaxation properties of the coupled Ni−C center are well interpreted by using the structural data and the exchange coupling constant obtained from the spectral simulations, which confirms the consistency of our analysis.

In contrast with systems where one of the interacting paramagnets is a radical species (Hirsh et al., 1992; Kodera et al., 1992), the structural organization of the coupled centers in hydrogenase could not be obtained from relaxation measurements alone. This is due to several reasons:

(i) Even at 4.2 K, some of the relaxation times of the coupled metal centers are very short, being close to the time resolution of the instruments, which precludes their accurate determination.

(ii) In the case of interacting metal centers, the anisotropy of the relaxation enhancement results not only from the dipolar interaction through the dependence upon the angle between the magnetic field and the intercenter vector (Hirsh et al., 1992) but also from the anisotropy of the **g**-tensors, which affects both the exchange (eqs 8 and 9) and dipolar (eqs 10 and 11) contributions. This adds a number of unknown parameters which cannot be determined from relaxation measurements alone.

Moreover, the contribution of the exchange interaction to the relaxation enhancement of the Ni−C center is quite important, being comparable to or larger than that of the dipolar interaction. This situation is not favorable to determine a spatial arrangement. For all these reasons, the numerical simulation of interaction EPR spectra recorded at several microwave frequencies appears as the best way to gain structural information on spin-coupled metal centers.

Preliminary data given by a low-resolution crystal structure of *D. gigas* hydrogenase have been recently published (Volbeda et al., 1993). According to these data, the four metal centers are roughly aligned, in a sequence Ni, [4Fe-4S], [3Fe-4S], [4Fe-4S], with intercenter distances of about 1.2 nm. The arrangement of the centers deduced from our analysis is in agreement with this description, which supports a sequential electron transfer mechanism from the catalytic site to the terminal acceptors of the enzyme. However, the intercenter distance we obtained is shorter (Table 1). It is important to note that our EPR study concerns the active state of the hydrogenase, while the crystallographic study

was performed in its oxidized, presumably inactive state. In addition, in the model we used to analyze the spin−spin interactions, the [4Fe-4S]$^{1+}$ cluster was considered as a point dipole whereas the magnetic moment carried by such a polynuclear center is strongly delocalized. A local spin model (Bertrand et al., 1994), which takes into account the electron spin distribution over the [4Fe-4S]$^{1+}$ cluster, should then be useful to refine the structural description of the active state of the *D. gigas* hydrogenase and to assign a valence state to the different iron ions of the [4Fe-4S]$^{1+}$ cluster. Further works are in progress with this aim.

REFERENCES

Adams, M. W. W. (1990) *Biochim. Biophys. Acta 1020*, 115−145.

Albracht, S. P. J., Van Der Zwaan, J. W., & Fontijn, R. D. (1984) *Biochim. Biophys. Acta 766*, 245−258.

Asso, M., Guigliarelli, B., Yagi, T., & Bertrand, P. (1992) *Biochim. Biophys. Acta 1122*, 50−56.

Bagyinka, C., Whitehead, J. P., & Maroney, M. J. (1993) *J. Am. Chem. Soc. 115*, 3576−3585.

Bertrand, P., Guigliarelli, B., Gayda, J. P., Setif, P., & Mathis, P. (1988) *Biochim. Biophys. Acta 933*, 393−397.

Bertrand, P., More, C., Guigliarelli, B., Fournel, A., Bennett, B., & Howes, B. (1994) *J. Am. Chem. Soc. 116*, 3078−3086.

Cammack, R. (1992) *Catalysis by Nickel in Biological System, in Bioinorganic Catalysis* (Reedijk, J., Ed.) Marcel Dekker, New York.

Cammack, R., & Cooper, C. E. (1993) EPR Spectroscopy of Iron Complexes and Iron-Containing Proteins, in *Methods in Enzymology, Metallobiochemistry, Part C* (Riordan, J., & Vallee, B., Eds.) Vol. 227, pp 353−384, Academic Press, San Diego.

Cammack, R., Patil, D., Aguirre, R., & Hatchikian, E. C. (1982) *FEBS Lett., 142*, 289−292.

Cammack, R., Patil, D., Hatchikian, E. C., & Fernandez, V. M. (1987) *Biochim. Biophys. Acta 912*, 98−109.

Cammack, R., Bagiynka, C., & Kovacs, K. L. (1989) *Eur. J. Biochem. 182*, 357−362.

Cammack, R., Williams, R., Guigliarelli, B., More, C. & Bertrand, P. (1994) *Biochem. Soc. Trans. 22*, 721−725.

Castner, T. G. (1959) *Phys. Rev. 115*, 1506−1515.

Chapman, A., Cammack, R., Hatchikian, E. C., McCracken, J., & Peisach, J. (1988) *FEBS Lett. 242*, 134−138.

Conover, R. C., Kowal, A. T., Fu, W., Park, J. B., Aono, S., Adams, M. W. W., & Johnson, M. K. (1990) *J. Biol. Chem. 265*, 8533−8538.

Coremans, J. M. C. C., Van der Zwaan, J. W., & Albracht, S. P. J. (1992) *Biochim. Biophys. Acta 1119*, 157−168.

Fernandez, V. M., Hatchikian, E. C., & Cammack, R. (1985) *Biochim. Biophys. Acta 832*, 69−79.

Fernandez, V. M., Hatchikian, E. C., Patil, D., & Cammack, R. (1986) *Biochim. Biophys. Acta 883*, 145−154.

Franco, R., Moura, I., LeGall, J., Peck, H. D., Huynh, B. H., & Moura, J. J. G. (1993) *Biochim. Biophys. Acta 1144*, 302−308.

Golbeck, J. H., McDermott, A. E., Jones, W. K., & Kurtz, D. M. (1987) *Biochim. Biophys. Acta 891*, 94−98.

Goodman, G. & Leigh, J. S., Jr. (1985) *Biochemistry 24*, 2310−2317.

Guigliarelli, B., Guillaussier, J., More, C., Setif, P., Bottin, H., & Bertrand, P. (1993) *J. Biol. Chem. 268*, 900−908.

Guillaussier, J. (1991) Thesis, Université de Provence, Marseille, France.

Hagen, W. R., & Albracht, S. P. J. (1982) *Biochim. Biophys. Acta 702*, 61−71.

Hatchikian, E. C., Bruschi, M., & LeGall, J. (1978) *Biochem. Biophys. Res. Commun. 82*, 451−461.

Hatchikian, E. C., Fernandez, V. M., & Cammack, R. (1990a), *FEMS Symp. 54*, 53−73.

Hatchikian, E. C., Traore, A. S., Fernandez, V. M., & Cammack, R. (1990b) *Eur. J. Biochem. 187*, 635−643.

He, S. H., Teixeira, M., LeGall, J., Patil, D. S., Moura, I., Moura, J. J. G., DerVartanian, D. V., Huynh, B. H., & Peck, H. D., Jr. (1989) *J. Biol. Chem. 264*, 2678−2682.

Hirsh, D. J., Beck, W. F., Innes, J. B., & Brudvig, G. W. (1992) *Biochemistry 31*, 532−541.

Kodera, Y., Takura, K., & Kawamori, A. (1992) *Biochim. Biophys. Acta 1101*, 23−32.

Kovacs, K. L., Seefeldt, L. C., Tigyi, G., Doyle, C. M., Mortenson, L. E., & Arp, D. J. (1989) *J. Bacteriol. 171*, 430−435.

LeGall, J., Ljungdahl, P. O., Moura, I., Peck, H. D., Jr., Xavier, A. V., Moura, J. J. G., Teixeira, M., Huynh, B. H., & DerVartanian, D. V. (1982) *Biochem. Biophys. Res. Commun. 106*, 610−616.

Lindahl, P. A., Kojima, N., Hausinger, R. P., Fox, J. A., Teo, B. K., Walsh, C. T., & Orme-Johnson, W. H. (1984) *J. Am. Chem. Soc. 106*, 3062−3064.

Mus-Veteau, I., Diaz, D., Gracia-Mora, J., Guigliarelli, B., Chottard, G., & Bruschi, M. (1991) *Biochim. Biophys. Acta 1060*, 159−165.

Saint-Martin, P., Lespinat, P. A., Fauque, G., Berlier, Y., LeGall, J., Moura, I., Teixeira, M., Xavier, A. V., & Moura, J. J. G. (1988) *Proc. Natl. Acad. Sci. U.S.A. 85*, 9378−9380.

Scott, R. A., Wallin, S. A., Czechowski, M., DerVartanian, D. V., LeGall, J., Peck, H. D., & Moura, I. (1984) *J. Am. Chem. Soc. 106*, 6864−6865.

Sorgenfrei, O., Klein, A., & albracht, S. P. J. (1993) *FEBS Lett. 322*, 291−297.

Tan, S. L., Fox, J. A., Kojima, N., Walsh, C. T., & Orme-Johnson, W. H. (1984) *J. Am. Chem. Soc. 106*, 3064−3066.

Teixeira, M., Moura, I., Xavier, A. V., DerVartanian, D. V., LeGall, J., Peck, H. D., Huynh, B. H., & Moura, J. J. G. (1983) *Eur. J. Biochem. 130*, 481−484.

Teixeira, M., Moura, I., Xavier, A. V., Huynh, B. H., Dervartanian, D. V., Peck, H. D., LeGall, J., & Moura, J. J. G. (1985) *J. Biol. Chem. 260*, 8942−8950.

Teixeira, M., Faugue, G., Moura, I., Lespinat, P. A., Berlier, Y., Prickril, B., Peck, H. D., Xavier, A. V., LeGall, J., & Moura, J. J. G. (1987) *Eur. J. Biochem. 167*, 47−58.

Teixeira, M., Moura, I., Xavier, A. V., Moura, J. J. G., LeGall, J., DerVartanian, D. V., Peck, H. D., & Huynh, B. H. (1989) *J. Biol. Chem. 264*, 16435−16450.

Van der Zwaan, J. W., Albracht, S. P. J., Fontijn, R. D., & Slater, E. C. (1985) *FEBS Lett. 179*, 271−277.

Van Der Zwaan, J. W., Albracht, S. P. J., Fontijn, R. D., & Mul, P. (1987) *Eur. J. Biochem. 169*, 377−384.

Volbeda, A., Piras, C., Charon, M. H., Hatchikian, E. C., Frey, M., & Fontecilla-Camps, J. C. (1993) *News Lett. Protein Crystallogr. 28*, 30−33.

Voordouw, G. (1992) *Adv. Inorg. Chem. 38*, 397−422.

Voordouw, G., Menon, N. K., LeGall, J., Choi, E. S., Peck, H. D., & Przybyla, A. E. (1989) *J. Bacteriol. 171*, 2894−2899.

BI9426423